Pseudo-capacitance of silver oxide thin film electrodes in ionic liquid for electrochemical energy applications

Oje, Alex.I.; Ogwu, A.A.; Mirzaeian, Mojtaba; Tsendzughul, Nathaniel; Oje, A.M.

Published in:
Journal of Science: Advanced Materials and Devices

DOI:
10.1016/j.jsamd.2019.04.003

E-pub ahead of print: 13/04/2019

Document Version
Peer reviewed version

Accepted Manuscript

Pseudo-Capacitance of Silver Oxide Thin Film Electrodes in Ionic Liquid for Electrochemical Energy Application

Alex.I. Oje, A.A. Ogwu, Mojtaba Mirzaeian, Nathaniel Tsendzughul, A.M. Oje

PII: S2468-2179(18)30292-2

DOI: https://doi.org/10.1016/j.jsamd.2019.04.003

Reference: JSAMD 220

To appear in: *Journal of Science: Advanced Materials and Devices*

Received Date: 31 December 2018

Revised Date: 1 April 2019

Accepted Date: 7 April 2019

Please cite this article as: A.I. Oje, A.A. Ogwu, M. Mirzaeian, N. Tsendzughul, A.M Oje, Pseudo-Capacitance of Silver Oxide Thin Film Electrodes in Ionic Liquid for Electrochemical Energy Application, *Journal of Science: Advanced Materials and Devices*, https://doi.org/10.1016/j.jsamd.2019.04.003.

Pseudo-Capacitance of Silver Oxide Thin Film Electrodes in Ionic Liquid for Electrochemical Energy Application

Alex.I. Oje [a], A.A. Ogwu [b], Mojtaba Mirzaeian [a], Nathaniel Tsendzughul [a], A.M Oje [a]

[a] School of Engineering and Computing,
University of the West of Scotland,
High Street, Paisley PA1 2BE, UK

[b] East Kazakhstan State Technical University,
Ust-Kamenogorsk, Republic of Kazakhstan

Corresponding Author: Alex.I. Oje, E-mail: ifeanyi.oje@uws.ac.uk

Abstract

The energy storage potential of silver oxide (Ag_2O) thin film electrodes, deposited via radio frequency reactive magnetron sputtering, were investigated in an ionic electrolyte (1-Ethyl-3-methylimidazolium bis(trifluoromethylsulfonyl)imide for supercapacitor application. X-ray diffraction (XRD), Raman spectroscopy, X-ray photoelectron spectroscopy (XPS) and Fourier Transform infrared spectroscopy (FTIR) tools were used to evaluate the structural and oxide phases present in the sputtered silver oxide thin film electrodes. The growth mode, morphology, surface area, wettability and surface energy of the deposited nano-structure silver oxide thin films were confirmed with scanning electron microscope (SEM), Brunauer-Emmetter-Teller (BET), goniometer and tensiometer. Furthermore, ion diffusion, Faradaic redox reactions and capacitance of the sputtered thin films exposed to 1-Ethyl-3-methylimidazolium bis(trifluoromethylsulfonyl)imide ionic electrolyte, were monitored with electrochemical impedance spectroscopy (EIS) and cyclic voltammetry (CV). SEM micrograph depicts that silver oxide thin films exhibit columnar growth mode, with wettability analysis revealing that Ag_2O thin film is hydrophilic, an excellent electrochemical behaviour indicator. Cyclic voltammetry measurements show that Ag_2O thin films exhibit a specific capacitance of 650 F/g at higher sputtering power, demonstrating its promising potential as an active electrode for supercapacitor application.

Keywords: Silver oxide, BET, EIS, cyclic voltammetry, pseudocapacitor

1. Introduction

The population of the world is expected to be on the increase as the years go by, therefore the use of energy is expected to increase with population density [1]. The fuel cell and battery technologies have been excellent storage systems for decades, however, the primary concern with them is that they are not suitable for burst power applications, due to their low power density output [2-4]. Storage devices like supercapacitors with their enormous power density and excellent cycle life are designed and engineered to solve the present and future energy storage problem [3-4]. The energy storage mechanism in supercapacitor could either be via charge separation in the Helmholtz double layer or reverse faradaic redox (oxidation-reduction) reaction on the electrode surface [5-6]. Supercapacitor performance depends on the kind of electroactive material used for the fabrication of the electrodes. This impacts the level of capacitive performance, energy density and power density of the supercapacitor [7]. The active electrode materials used for supercapacitor processing are grouped into carbon, conducting polymers and transition metal oxide-based materials, with carbon-based materials predominantly used for processing EDLC type of supercapacitors. The conducting polymers and transition metal oxide materials are mainly used for the pseudocapacitor kind of supercapacitor, while the combination of the three materials is for processing the composite electrodes for hybrid supercapacitors. Activated carbon is one the most investigated carbon materials for EDLC because of their low cost, high surface area and good electrical properties, but yields lower energy density and are unsuitable for high-temperature use [8]. Transition metal oxide-based electrodes such as ruthenium oxide (RuO_2) [9-10], manganese oxide (MnO_2) [11], vanadium oxide (V_2O_5) [12], Iron oxide (Fe_2O_3) [13], solves the problem that carbon base materials are faced by [8]. Despite ruthenium oxide excellent electrochemical performance, its toxicity to the environment and its high cost hinders its wider commercialization as electroactive material for supercapacitor applications. Investigating alternative base material such as silver oxide that is cheap and has the potential to exhibits electrochemical behaviour close to that of ruthenium oxide is the aim of this research. Silver forms different oxide phases such as AgO, Ag_3O_4, Ag_4O_3, Ag_2O_3 and Ag_2O with silver oxide (Ag_2O) been the most stable amongst them [14]. The ability for silver oxide to change and adopt different oxidation states (+1, +2), facilitates the energy storage ability of Ag_2O. Silver oxide has previously been studied by various researchers for different applications such as anti-microbial agent [15-17], due to the release of silver ion (Ag^+), reactive oxygen spices (ROS) and the hydroxyl group, which are produced from redox

reaction. Fuji et al. [18] and Kim et al. [19] reported silver oxide widely used in optical disk storage due to their photoactivation properties. Her et al. [20] integrated silver oxide thin films into super resolution near field structures, for optical memory applications. Silver oxides nanostructured particles have also served as a protective coating material, to stop the degradation of zinc oxide-based photodetectors [21]. Silver oxide thin film coating has been deployed successfully as a substrate for surface-enhanced Raman spectroscopy for molecular level detection [22]. Silver oxide nanomaterials have been studied and found to be highly conductive, making them suitable for battery cell applications [23-25]. Porous morphology, good conductivity, good thermal stability and reasonable wettability are some of the characteristics [23-29], attributed to silver oxide, making it a promising electroactive material for pseudocapacitor applications. In this work, the energy storage potential of Ag_2O thin films produced by reactive magnetron sputtering was investigated in ionic electrolyte to determine its electrochemical performance and suitability for supercapacitor application.

2. Experimental Investigation

The thin film disposition parameters, structural characterization and electrochemical measurement details are described by Oje et al. [28]. The charge-discharge measurement was carried out for 10000 cycles for an applied current and voltage window of 10mA and 1V respectively. Furthermore, the following voltage range was used for the cyclic voltammetry analysis -1000mV to 1000mV, for scan rate of 2mV/s, 5mV/s and 10mV/s respectively.

3. Results and Discussion

3.1 XRD, Raman, FTIR and XPS results

The diffraction peaks for the crystal structure of Ag_2O thin films sputtered on microscope glass slides, were established using the standard international centre for diffraction data card number (ICCD CARD number: 041-1104). The Braggs peaks on the Ag_2O thin films deposited at 250W, 300W, 350W and at oxygen flow rates of 10sccm reveal that the deposited silver oxide thin films are crystalline as shown in Figure 1a, with peaks at (111), (002) and (200) crystal planes, reflecting silver oxide cubic structure. The sharp Bragg peak on the (200) crystal planes of Ag_2O 350W 10sccm thin film, Reddy et al. [30] and Hammad et al. [31], attribute to increase in crystal grain size as deposition power increases. The crystal grain orientation of the silver oxide changes from (111) to (200) crystal plane, an indication that the sputtered silver oxide thin film is nonhomogeneous [29, 31-33]. This also suggests that the non-uniformity of the sputtered Ag_2O thin films increase with deposition power.

Furthermore, Ingham et al. [34], reported that the shift in the 2θ angles of the crystal planes of silver oxide in Figure 1a is due to the sputtered Ag_2O thin films nonhomogeneous and columnar growth structure. The packing arrangement in the cubic structure of silver oxide deposited at all the conditions are in cubic shape at the (111), (002) and (200) crystal planes [29,32,35,36-38]. This gives rise to the cubic interstitial site, where electrolyte diffusion can take place, thereby encouraging redox reaction process.

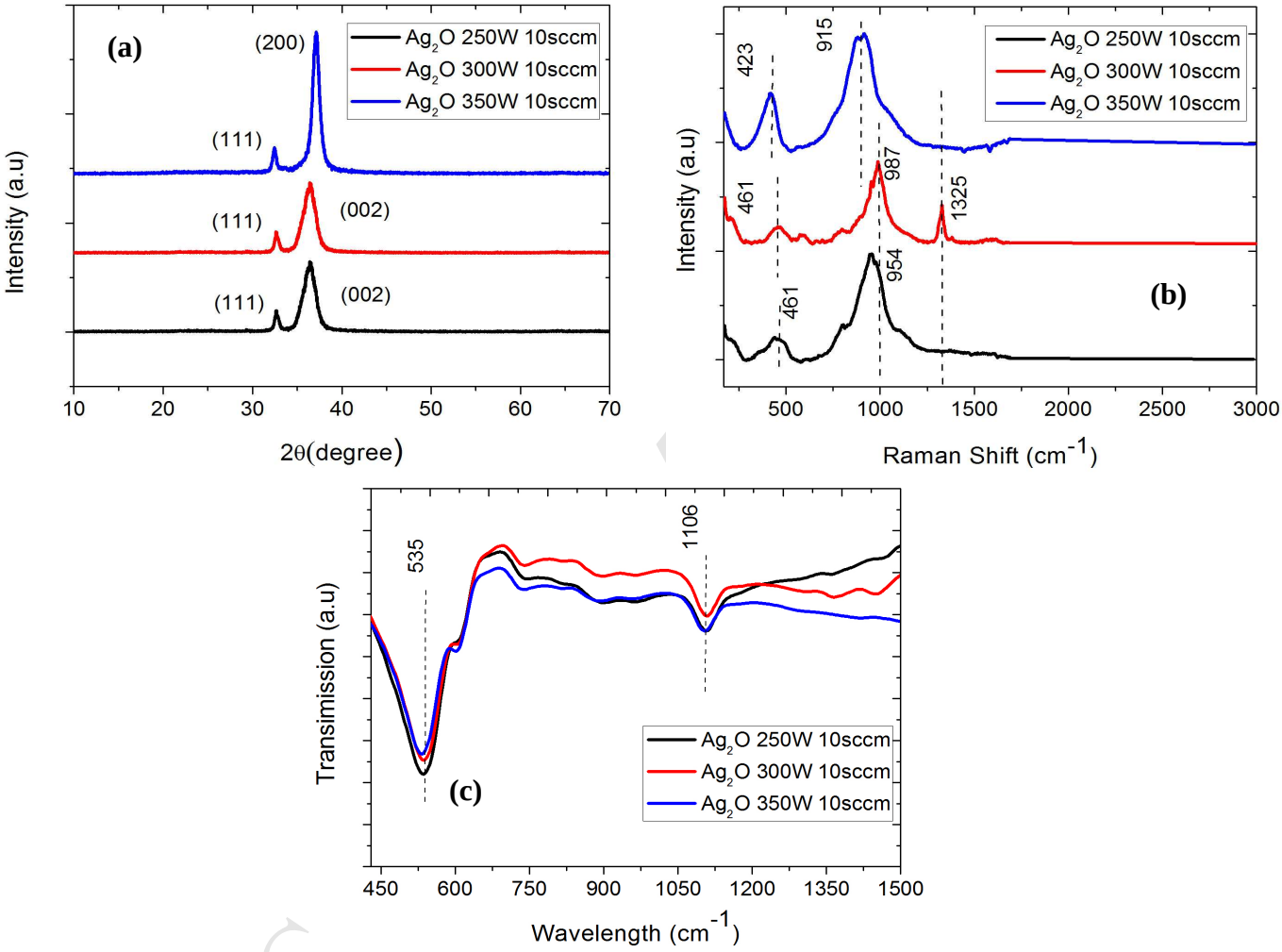

Figure 1: (a) XRD (b) Raman and (c) FTIR results of Ag_2O thin films deposited at 250W, 300W and 350W at oxygen flow rate of 10sccm

The Raman spectroscopy of Ag_2O thin films shown in Figure 1b (250W, 300W and 350W) for oxygen flow rate of 10sccm exhibits Raman bands at 423 cm^{-1}, 461 cm^{-1}, 915 cm^{-1}, 954 cm^{-1}, 987 cm^{-1} and 1325 cm^{-1}. The Raman shift at 423 cm^{-1} and 461cm^{-1} are due to the stretching mode of silver oxide on the (111) crystal lattice, where the oxygen molecules

occupy the cubic interstitial holes [34,39-40]. There is a shift in the Raman peaks as the deposition power increases for silver oxide thin films produced at radio frequency power of 250W, 300W and 350W at 10sccm oxygen flow rate. This is due to the ability of the grain boundaries trapping more oxygen molecules at higher deposition power for the silver oxide thin film deposited at 350W 10sccm. Martina et al. [41], attribute the 915 cm^{-1}, 954 cm^{-1} and 987 cm^{-1} Raman spectra peaks to chemosorbed atomic/molecular oxygen species end bond on deposited Ag_2O thin films with (002) and (200) crystal lattices being the preferred cubic interstitial sites for the oxygen molecules. Furthermore, the 1325 cm^{-1} peaks are the sums of the Ag-O (270 cm^{-1}) and O-O (930 cm^{-1}) stretching mode, giving rise to superimposed vibrational mode.

Figure 1c shows the deposited silver oxide thin films FTIR spectra, with peaks at 535 cm^{-1} and 1106 cm^{-1}. The 535 cm^{-1} peak is the lattice vibration mode of silver oxide, due to the Ag-O-Ag bonding and the 1106 cm^{-1} is attributed to O-H stretching vibration mode. This vibration lattice peak is within the FTIR vibrational mode reported in various literature reviews on silver oxide FTIR spectrum [42-45]. There is a continuous increase in the FTIR peak intensity as the deposition power increases for Ag_2O thin films prepared at (250W, 300W and 350W) as shown in Figure 1c. This is due to the ability of sputtering gases to acquire more excitation energy at higher power and dislodge more silver atoms from the target, thereby increasing the deposition rate, the films thickness and crystal size of the deposited Ag_2O thin films as forward power increases. Silver oxide vibrational lattice peak at 535cm^{-1} arises from the (002) and (200) crystal planes. The cubic interstitial site on the crystal planes provides spaces for the diffused oxygen molecules to bond with the silver atoms. This bonding at this cubic interstitial site leads to Ag-O-Ag vibrational lattice and the eventual FTIR silver oxide peak at 535 cm^{-1}. At higher deposition power, more intense silver oxide films are produced and this confirms the XRD and Raman spectroscopy findings.

XPS was used to study the elemental constituent of the prepared silver oxide thin films and other elements they are bonded to. The binding energy of 368.3eV and 531.8 eV in Figure 2a, Figure 2b indicate the presence of Ag (Ag 3d) and oxygen (O 1s) [36,46-48] in the sputtered sample. The bonding of Ag-O in the deposited thin film sample is evidenced in the O1s spectra, at 531.8 eV binding energy [36,49-52], which stems from subsurface oxygen formation. The survey spectrum in Figure 2c reveals the presence of silver metal and atomic oxygen at a binding energy of 390 eV and 560 eV. Kaspar et al. [46], reported similar binding

energy for metallic silver co-deposited with atomic oxygen. The XPS binding energies at 368.3eV and 531.8 eV are within the standard values for silver and oxygen atoms.

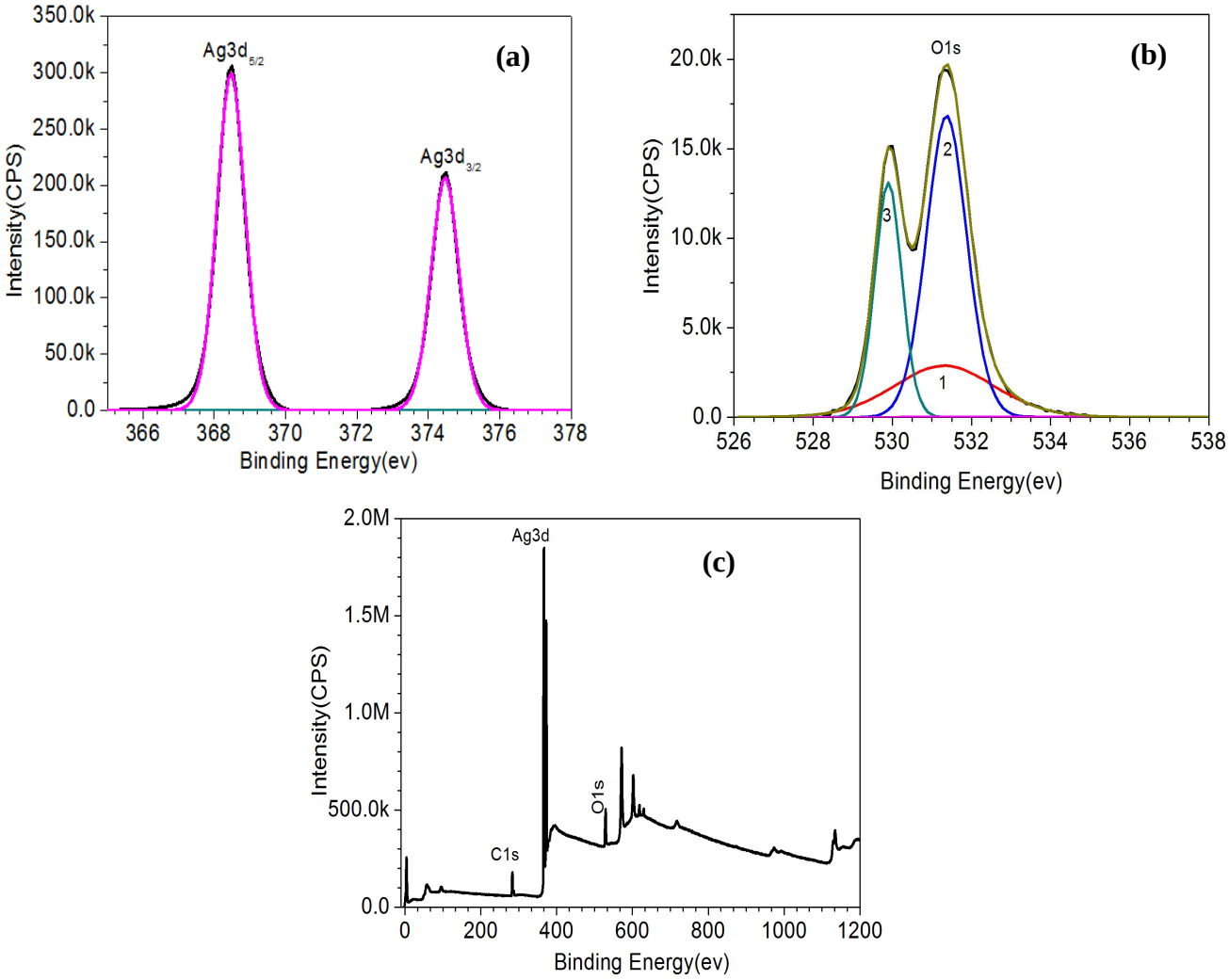

Figure 2: XPS of silver oxide (a) Ag 3d (b) O1s and (c) survey spectrum

3.2 SEM Results and BET Surface Area.

A scanning electron microscope (SEM) was deployed to reveal the microstructural information of the produced Ag_2O thin film electrodes. The top surface view of the Ag_2O thin films SEM micrograph in Figure 3a, Figure 3b and Figure 3c, reveal agglomeration of silver oxide crystals as shown on films prepared at 250W. As deposition power increased, Volmer-Weber growth mode mechanism (island growth mode) can be seen on the top view micrographs of the sputtered Ag_2O thin films, similar to Rebelo [36] findings. The prepared silver oxide thin films crystal size increases with sputtering power, which Agasti et al. [52] attribute to the trapping of more atoms of oxygen inside the grain boundaries as deposition power increases. The prepared Ag_2O thin film electrodes at oxygen flow rate of 10sccm and

sputtering power (250W, 300W and 350W) exhibited columnar growth mode from the cross-sectional view in Figure 3. The columnar growth structure, island formation and segregation of silver and oxygen atoms lead to void creations. This island growth exhibited by silver oxide thin films, allow the molecules to be bonded strongly to each other, enabling the clustering of the atoms. As the deposition power increases, the pores on the silver oxide thin films become more pronounced, and atoms agglomerate forming a larger island. Rebelo et al. [36], believes this is due to the growth of stable nuclei to the maximum and the ability of more oxygen molecules to diffuse at higher deposition power. The improved roughness and mesopores as deposition power increases, enhance conductivity, improves ion diffusion and facilitates the redox reaction [31, 53-59]. This is an indication that Ag_2O 350W 10sccm will offer more surface area for electrode/electrolyte interaction, resulting in higher specific capacitance.

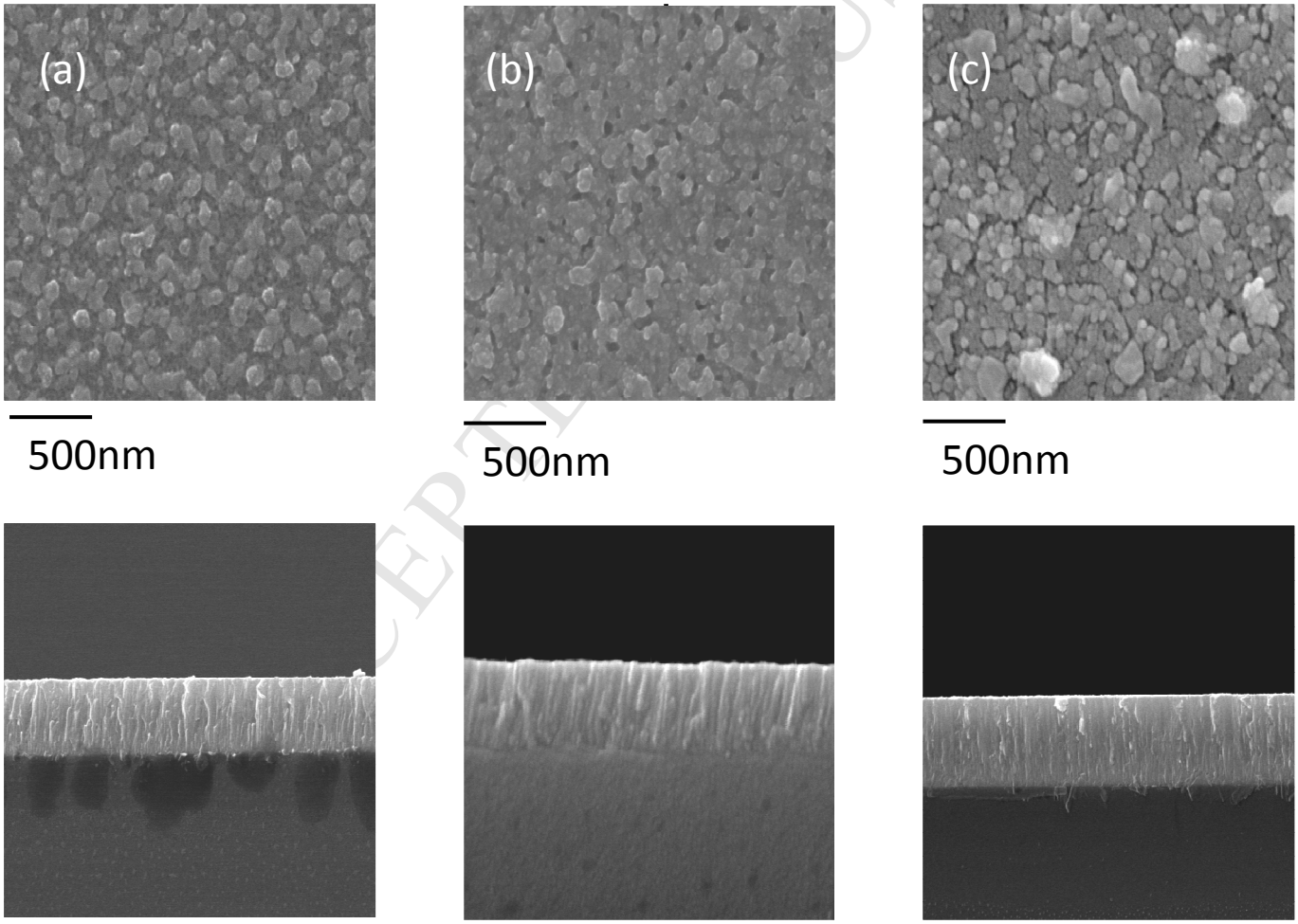

Figure 3: SEM images of silver oxide thin films deposited at 10sccm showing top and cross-sectional view (a) 250W (b) 300W and (c) 350W

BET analysis was used to evaluate the surface area and the average pore size of the deposited silver oxide thin films and the results presented in Table 1. The BET experimental analysis reveals that the surface area and average pore size of the sputtered Ag_2O thin films, increases as deposition power increases as depicted in Table 1. Dimitrijević et al. [60] and Agasti et al. [61], attributes this to ions been more energetic as sputtering power increases from 250W to 350W, resulting in bigger surface area and more probability of nanoclusters. Arjomandi et al. [62] suggest that higher surface area allows faster transport through the electrolyte ions and this increases the supercapacitor performance [63], supporting SEM results. Furthermore, Zhao et al. [64], reported that electrode surface area and pore size are directly connected to specific capacitance, with more surface area presenting more active sites for interfacial faradaic reaction and charge storage. An indication that energy density can be improved by increasing specific capacitance, a direct impact of surface area and pore size improvement.

Table 1: BET surface area and average pore size of silver oxide thin films

Deposition Power (W)	**BET surface area (m^2/g)**	**Pore Size (nm)**
250	26.19	9.41
300	38.21	12.49
350	41.04	15.03

3.3 Wettability and Surface Energy Analysis

Figure 4 shows the wettability analysis of the Ag_2O thin film electrodes conducted using contact angle measurement. The results of Ag_2O thin films static and dynamic plot show that silver oxide is hydrophilic, with all the contact angle less than 90^o, signifying good wettability as shown in Figure 4. Figure 4a shows a continuous decrease in the static contact angle of Ag_2O thin films as deposition power increases. An indication that silver oxide electrode/electrolyte interaction improves as sputtering power increases. Figure 4b reveals similar results for contact angle measurement using dynamic techniques, further confirming the hydrophilic nature of the deposited thin films. The advancing and the receding contact angle differences give rise to contact angle hysteresis, due to the change in the surface configuration (SEM) of the sputtered Ag_2O thin films [65-68]. This is an indication of electrolyte intrusion into the silver oxide thin films mesopores. Ag_2O 350W 10sccm sputtered

thin film electrode yields smaller contact angle hysteresis in contrast to the Ag_2O thin films prepared at 250W and 300W respectively. An indication of Ag_2O 350W 10sccm higher degree of wetting and diffusion of the electrolyte into the microstructure of the electrode [65-67]. Wettability and electrolyte penetration lead to improved charge transfer process across the electrode-electrolyte, thereby encouraging the pseudocapacitance process. The cubic interstitial sites [68], provide the sites for electrolyte penetration and diffusion for the electrochemical performance of the deposited thin films. SEM micrograph and wettability results of silver oxide thin films suggest that Ag_2O 350W 10sccm is the most viable electrode material for pseudocapacitor application.

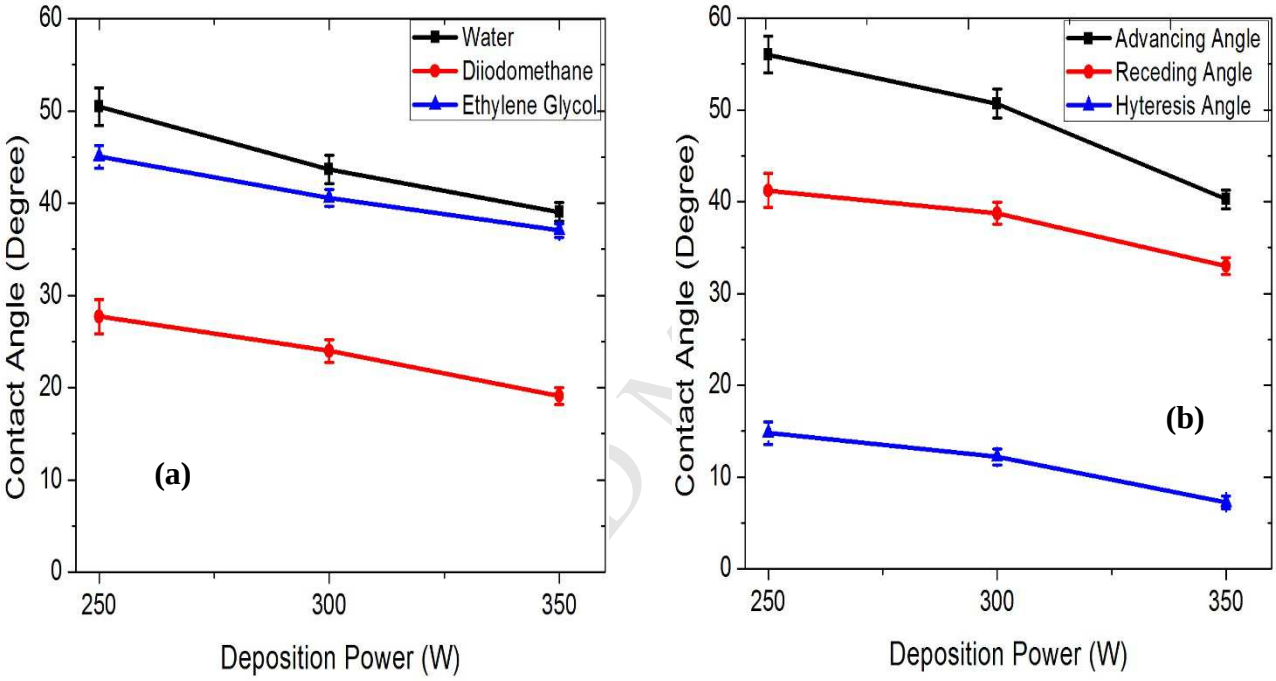

Figure 4: Contact angle graphs of Ag_2O thin films (a) static, (b) dynamic

Surface energy analysis was performed using three approaches namely: Fowkes, Wu and acid-base approach. Figure 5 and Table 2 reveal that, the total surface energy (γ^{total}) of the Ag_2O thin films increased as deposition power increases [29]. The wettability of the deposited Ag_2O thin films depends on the overall contribution of the polar component γ^{p} to the entire surface energy. The higher the polar component contribution to the overall surface energy, the better the wettability of the films [69] as shown in Figure 5a, 5b and Table 2. Silver oxide thin film sputtered at 350W, show higher polar component contribution to the

total surface energy. This is an indication of its excellent electrode/electrolyte interaction resulting in lower contact angle, supporting the contact angle results. The sputtered Ag_2O 350W 10sccm excellent wettability is evident in the magnitude of the polar components in the Fowkes, Wu and acid-base surface energy depicted in Figure 5a, 5b and Table 2.

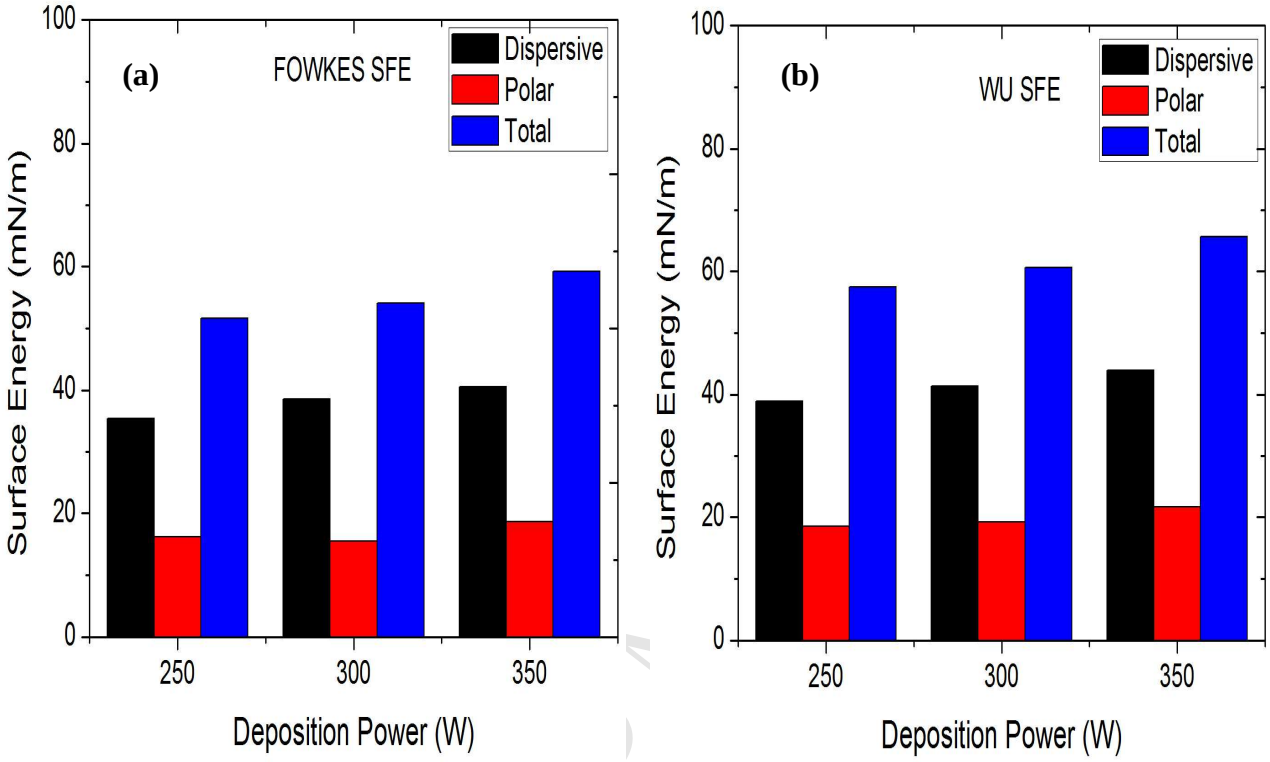

Figure 5: Ag_2O thin films Surface Energy using (a) Fowkes and (b) Wu approach

Table 2: silver oxide thin films surface energy

	Surface Energy (mN/m)								
	Fowkes			Wu			Acid-Base		
Power (W)	γ^d	γ^p	γ^{total}	γ^d	γ^p	γ^{total}	γ^{lw}	γ^{AB}	γ^{total}
250	35.43	15.14	50.57	38.86	18.57	57.43	46.94	-6.04	40.90
300	38.56	15.56	54.12	41.38	19.24	60.62	49.08	-4.10	44.98
350	40.51	18.67	59.18	43.98	21.64	65.62	50.80	-2.18	48.62

3.4 Electrochemical Impedance Spectroscopy (EIS)

Figure 6 shows the Electrochemical Impedance Spectroscopy results of Ag_2O thin films in an ionic electrolyte, presented using Nyquist and Bode plot. The sputtered Ag_2O thin film electrode at 350W 10sccm displays Warburg diffusion line 45^o to the Z-axis, an ion intercalation process, which reveals the pseudocapacitive characteristics of the Ag_2O thin films produced at 350W 10sccm [70-73]. The electron charge transfer process a second part of the ion intercalation, reveals lower impedance value for Ag_2O 350W 10sccm, making it the most conductive silver oxide prepared for this investigation. This can be linked to the Ag_2O 350W 10sccm sample offering more surface area and more pore size for ion diffusion, which improves the electrochemical performance. There is a shift in Ag_2O 250W 10sccm and Ag_2O 300W 10sccm electrodes, from the 45^o spectra line to the Z axis as shown in Figure 6a. These variations, Criado et al. [74] linked to non-uniformity of Ag_2O thin films coating and the reflective boundary condition at the electrode. The Bode plot in Figure 6b further supports the Nyquist plot finding, with Ag_2O 350W 10sccm thin film again exhibiting lower impedance compared to 250W 10sccm and 300W 10sccm electrodes. The equivalent circuit model of the various sputtered Ag_2O thin film electrodes was simulated using a Z-view software. Silver oxide thin films prepared at 250W 10sccm, 300W 10sccm and 350W 10sccm correspond to charge transfer resistance of 32.09Ω, 28.72Ω and 22.14Ω respectively. The reduced charge transfer resistance offered by silver oxide thin film processed at 350W 10sccm indicate better ionic electrolyte transport via the electrolyte/electrode interface. Pawar et al. [75], reported that the lower impedance of silver oxide thin film sputtered at 350W 10sccm (22.14Ω) is an indication of its high conductivity and the ability to offer more surface area for ion diffusion for better electrochemical supercapacitor performance [76]. The wettability analysis further explains this, where Ag_2O 350W 10sccm showed the lowest contact angle, due to the dominant contribution from the polar component of the total surface energy. This suggests that the surface of the Ag_2O thin film deposited at 350W 10sccm had maximum interaction with the three probing liquids, used during the contact angle analysis. This leads to lower contact angle and higher surface energy values as depicted in Figure 4 and Figure 5 respectively.

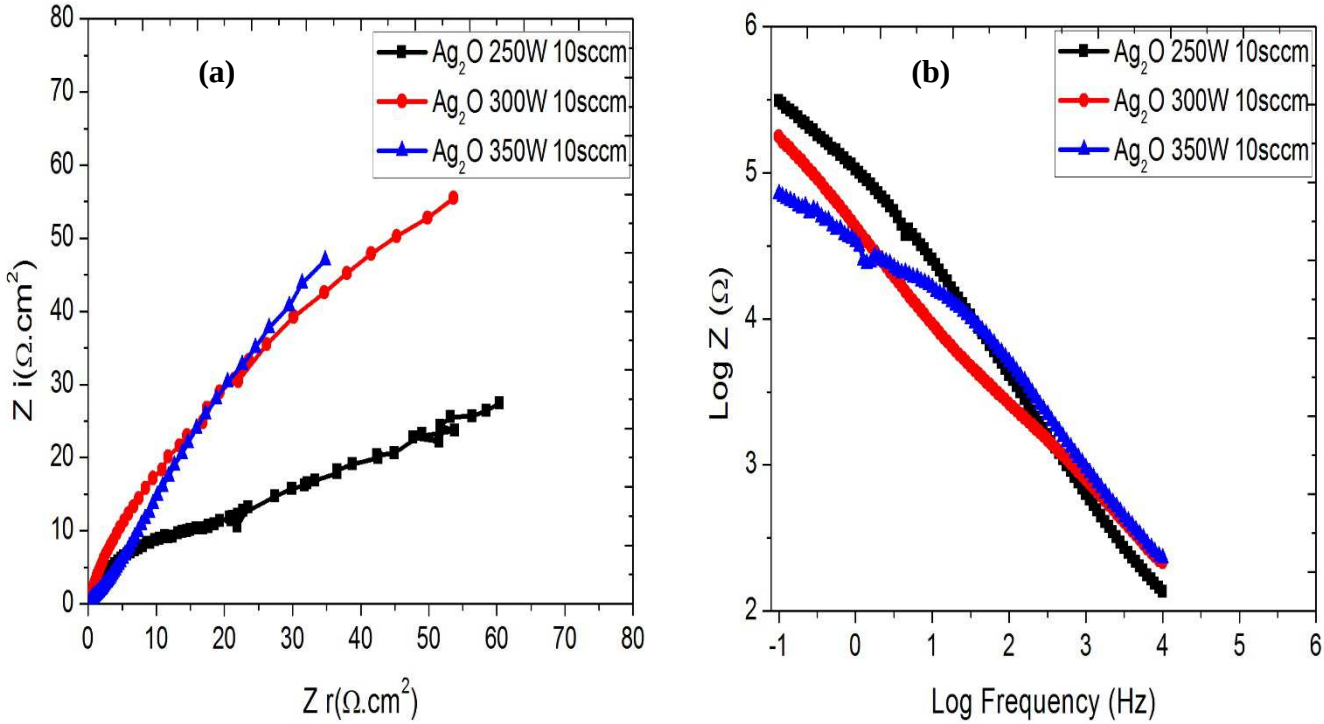

Figure 6: EIS of Ag_2O thin films using (a) Nyquist and (b) Bode plot

3.5 Charge-discharge

Figure 7 Show the charge-discharge curves of silver oxide thin films deposited at a constant oxygen flow rate of 10sccm and varying power of 250W, 300W and 350W. The mirror-like charge-discharge curves confirm the pseudocapacitance property of silver oxide due to Faradaic redox reaction. Silver oxide thin film deposited at 350W 10sccm show a better voltage window utilization, an indication of it's potential to store more charge compared to Ag_2O 250W 10sscm and Ag_2O 300W 10sscm respectively. This actually stems from Ag_2O 350W 10sscm morphology offering more surface area and pore for interfacial faradaic reaction and charge storage [64]. The bigger surface area and pore size of Ag_2O 350W 10sscm pave the way for more electrolyte intrusion, spreading and an improved electrode/electrolyte interaction. This further allows more charge transfer process across the sputtered Ag_2O 350W 10sscm electrode, thereby encouraging redox reaction process. Furthermore, the stability of the prepared silver oxide thin films was tested for 10000 cycles, at 10mA applied current, for voltage window of 1V. Figure 7 (a, b and c) show the initial and last ten cycles charge-discharge measurements for the three-silver oxide thin film electrodes, with a 2% drop between the initial and the last 10 cycles potential for the entire 10000 cycles.

An indication of the excellent stability of the three silver oxide electrodes for supercapacitor application and an improvement to what has been reported in the literation on the voltage window drop [28].

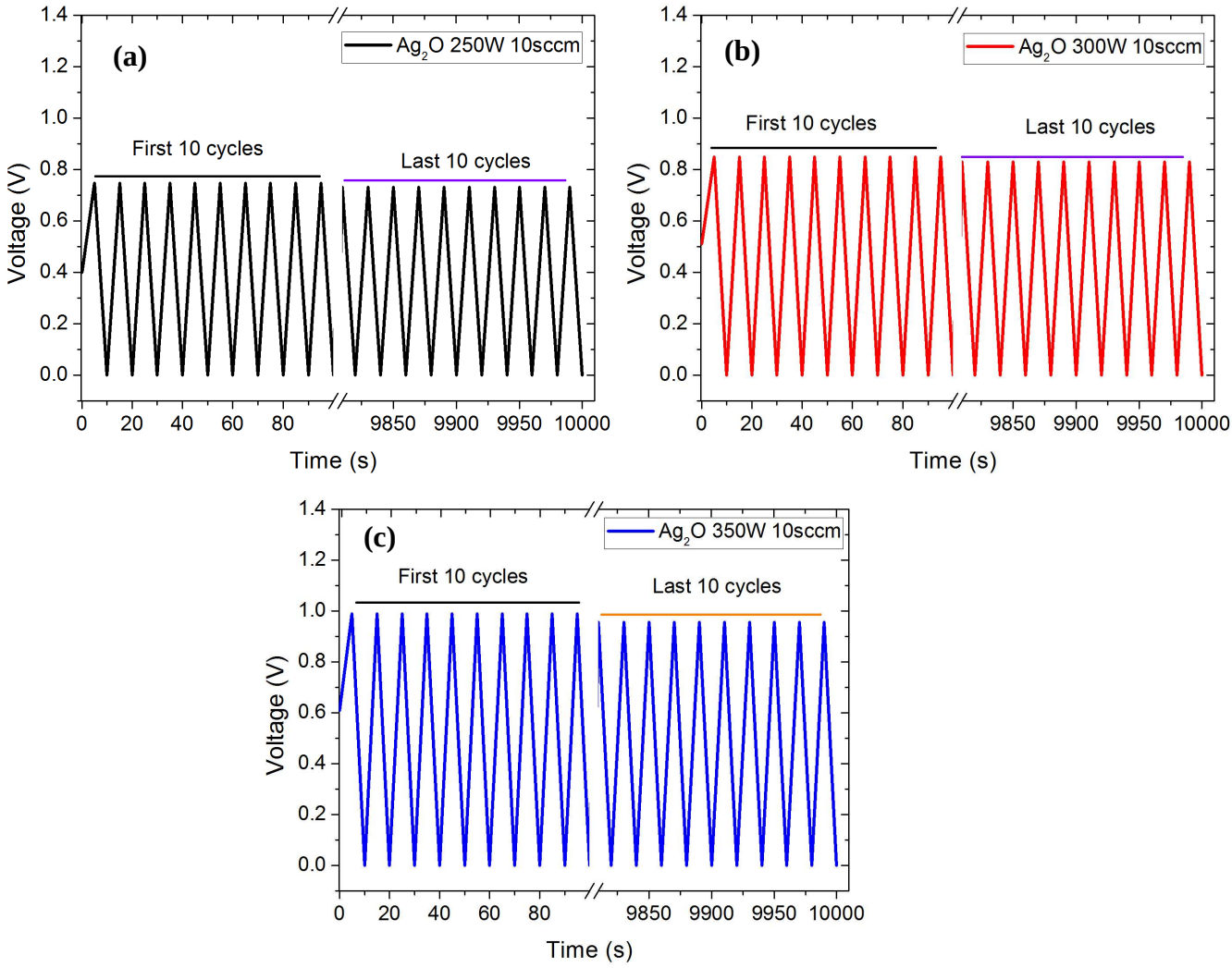

Figure 7: silver oxide thin films first and last 10 cycles charge discharge for 10000 cycles at (a) 250W (b) 300W (c) 350W 10sccm respectively

3.6 Cyclic Voltammetry

Figure 8 shows the cyclic voltammetry of silver oxide thin films in 1-Ethyl-3-methylimidazolium bis(trifluoromethylsulfonyl)imide ionic solution with two redox peaks. The anodic and cathodic peaks are due to the oxidation and reduction of silver oxide thin films by the $[N(Tf)2]^-$ anion and $[EMIM]^+$ cation of the ionic liquid (1-Ethyl-3-methylimidazolium bis(trifluoromethylsulfonyl)imide [77-78]. There is an increase in CV curves of silver oxide thin films sputtered at 350W 10sccm as deposition power increases,

with redox peak voltages at -0.6 to -0.8V and at +0.6 to 0.8V, an indication of charge transfer process taking place. Abedin et al. [79], attributes this increase in peak current to the oxidation of the $[EMIM]^+$ cation, a reduction reaction product. These redox peak voltages are within the standard oxidation-reduction potential reported by Amor et al. [80] on silver oxide redox peak. Nanostructure silver oxide film prepared at 350W 10sccm has higher peak current density compared to silver oxide thin films sputtered at 250W 10sccm and 300W 10sccm as shown in Figure 8. This is because at 350W 10sccm, the deposited silver oxide electrode offers more surface area for electrolyte/electrode interaction, resulting in better capacitance performance. Using equation 1, the specific capacitance of the various prepared Ag_2O can be determined [81],

$$C_s = \frac{1}{m\, v\, (V_c - V_a)} \int_{V_a}^{V_c} I(V)\ dV \qquad (1)$$

Where v is the potential scan rate (mV/s), $(V_c - V_a)$ is the potential range, I stands for the current response and m the weight of the electrode. Using equation 1, specific capacitance of Ag_2O at 250W 10sccm at 2mV/s, 5mV/s and 10mV/s are 617 F/g, 519 F/g and 429 F/g respectively. At a scan rate of 2mV/s, 5mV/s and 10mV/s, silver oxide thin films sputtered at 300W 10sccm gave specific capacitance of 623 F/g, 540 F/g and 489 F/g respectively. Furthermore, cyclic voltammetry analysis of silver oxide thin films prepared at 350W 10sccm, resulted in specific capacitance of 650 F/g, 591 F/g and 531 F/g, at a scan rate of 2mV/s, 5mV/s and 10mV/s respectively. It is obvious from the specific capacitance calculation that the scan rate affects the oxidation/ reduction peak current height and the shape of the curve, with a scan rate of 10mV/s offering more peak current but less capacitance. This is because a limited number of ions are allowed to diffuse into the microstructure of the silver oxide thin films at a higher scan rate (10mV/s), reducing the redox reaction process [80]. The pseudocapacitance behaviour is revealed on the cathodic and anodic sides of the CV curves, by the peak current at each of voltage level. An indication of valuable utilization of the silver oxide material by the ions from the electrolyte via the redox reaction process. Ag_2O thin film prepared at 350W 10sccm yields higher specific capacitance compared to silver oxide thin films at 250W 10sccm and 300W 10sccm

respectively. The produced Ag_2O 350W 10sccm higher specific capacitance can be attributed to it's better morphological arrangement, bigger surface area, pore size and reduced charge transfer resistance as depicted in the SEM, BET and EIS results. The reported specific capacitance in this research is an improvement to 275.50 F/g and 530 F/g reported by oje et al. and Elaiyappillai et al. [28, 82], on silver oxide-based supercapacitors. The measured specific capacitance from cyclic voltammetry analysis for silver oxide thin films still depends on the electrode processing method, surface area, pore size and ion size [28, 82-84].

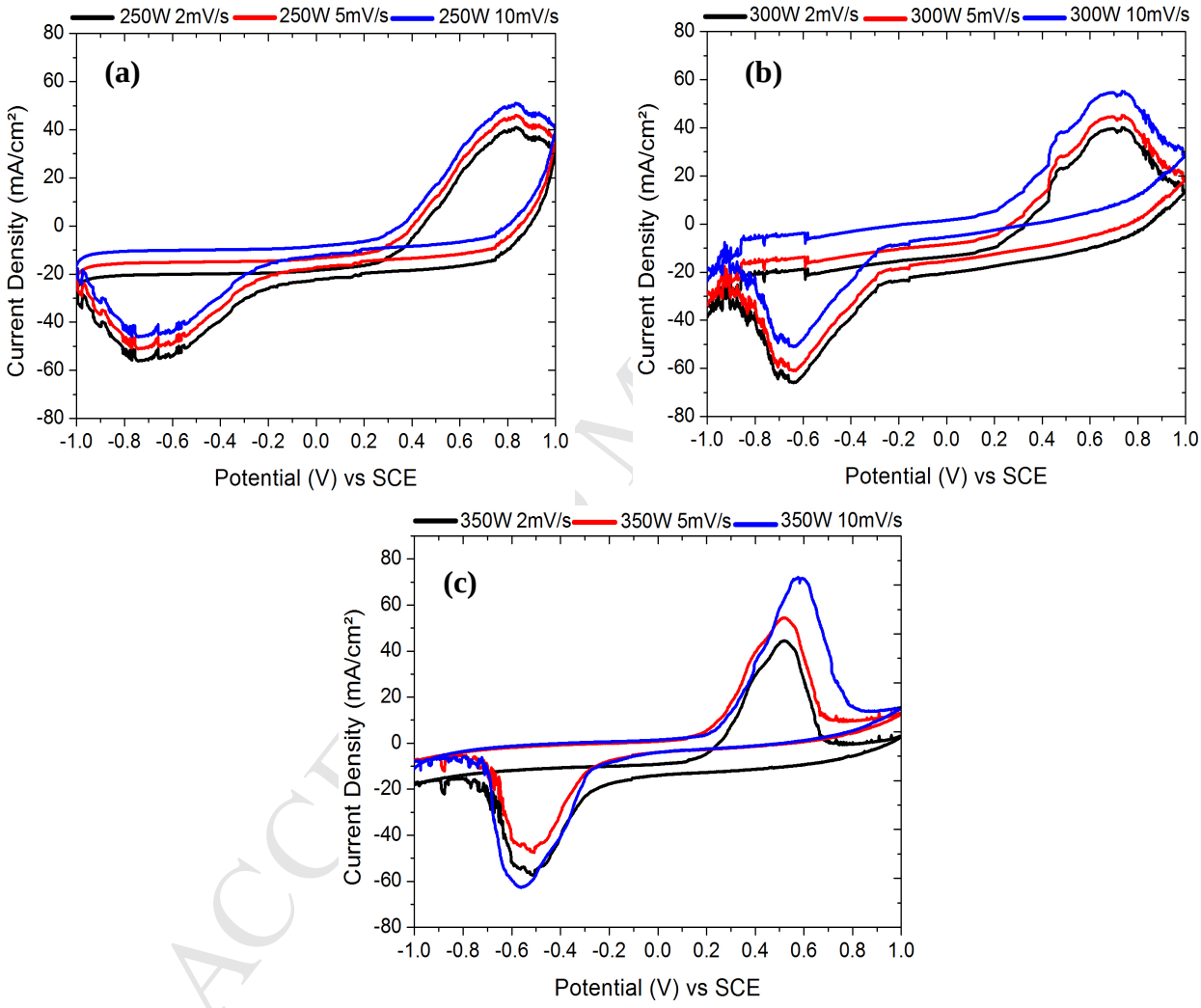

Figure 8: silver oxide thin films CV in ionic solution at 10sccm (a) 250W (b) 300W (c) 350W at scan rate of (2mV/s, 5mV/s, 10mV/s)

Conclusions

In this research, radio frequency magnetron sputtering was successfully used to fabricate thin film electrodes based on nanostructure silver oxide materials, for energy storage application, supercapacitor to be precise. XRD, Raman spectroscopy, XPS and FTIR reveals that the oxide phases belong to silver oxide. The scanning electron micrograph indicates that the deposited silver oxide thin films exhibited Volmer-Weber mechanism growth mode, with film roughness and pores increasing with deposition power. The BET surface area measurement shows that as the deposition power increases the surface area and average pore size, with Ag_2O thin films prepared at 350W exhibiting better wettability, an indication of strong interaction between the electrode/electrolyte.

Furthermore, electrochemical impedance spectroscopy, charge-discharge and cyclic voltammetry in (1-Ethyl-3-methylimidazolium bis(trifluoromethylsulfonyl)imide reveal that Ag_2O thin films produced at 350W, possesses lower charge transfer resistance, good cycle life and a specific capacitance of 650 F/g at 2mV/s scan rate. The enhance specific capacitance at higher deposition power can be linked to silver oxide thin films sputtered at 350W 10sccm offering more surface area, more pore size and reduced charge transfer resistance for oxidation-reduction reaction.

Supercapacitor plays important role in energy storage technology because of the high-power boost it offers as a stand-alone or complementary energy storage device in hybrid cars, trains, space tools, airplanes, windmills, cranes and consumer electronic gadgets. The specific capacitance of 650 F/g offered by silver oxide thin film, demonstrates its electrochemical potential to be used as an active electrode for supercapacitor processing. This is extremely important for energy recovery systems such as car dynamic braking systems, where supercapacitors excellent life cycle, paves the way for it to be used to extend the lifespan of battery storage technology.

Funding. No funding was received for this research.

References

1. Inamullah Haneef, Faisal Hussain Memon, Energy crisis and it's statistics: SPE Annual Technical Conference, 25-26 November 2014, Islamabad, Pakistan.
2. R. kotz, M. Carlen, Principles and applications of electrochemical capacitors: Electrochimica Acta 45 (2000) 2483–2498.
3. Feng L., Zhu. Y, Ding. H, Recent progress in nickel-based materials for high-performance pseudocapacitor electrodes: Journal of Power Sources 267 (2014) 430-444.
4. Wang. G, Zhang. L, Zhang J, A review of electrode materials for electrochemical supercapacitors: Chemical Society Reviews 41 (2012) 797-828.
5. Peter J. Hall, Mojtaba Mirzaeian, S. Isobel Fletcher, Energy storage in electrochemical capacitors-designing functional materials to improve performance: Energy Environ Sci 3 (2010) 1238-1251.
6. M. Winter, R.J. Brodd, What are batteries, fuel cells, and supercapacitors?: Chemical Reviews 104 (2004) 4245-4269.
7. Mojtaba Mirzaeian, Qaisar Abbas, Abraham Ogwu, Electrode and electrolyte materials for electrochemical capacitors: International Journal of Hydrogen Energy 42 (2017) 25565 – 25587.
8. B.E Conway. Electrochemical Supercapacitors: Scientific Fundamentals and Technological Applications, Kluwer Academic/Plenum Publishers, New York, 2nd Edition, 1999.
9. V.D. Patake, C.D. Lokhande, O.S. Joo, Electrodeposited ruthenium oxide thin films for supercapacitor: effect of surface treatments: Applied Surface Science 255 (2009) 4192-4196.
10. Pengfei Wang, Hui Liu, Yuxing Xu, Yunfa Chen, Supported ultrafine ruthenium oxides with specific capacitance up to 1099 F g-1 for a supercapacitor: Electrochimica Acta 194 (2016) 211– 218.
11. J. Liu, J. Essner, J. Li, Hybrid Supercapacitor Based on Coaxially Coated Manganese Oxide on Vertically Aligned Carbon Nanofiber Arrays: Chem. Mater. 22 (2010) 5022-5030.
12. S. Beke, A review of the growth of V2O5 films from 1885 to 2010: Thin Solid Films 519 (2011) 1761-1771.
13. X. Cheng, X. Gui, Z. Lin, Three-dimensional α-Fe_2O_3/carbon nanotube sponges as flexible supercapacitor electrodes: J. Mater. Chem. A 3 (2015) 20927-20934
14. M. Bielmann, P. Schwaller, P. Ruffieux, AgO investigated by photoelectron spectroscopy evidence for mixed valence: Physical Review B 65 (2002) 235431.

15. I. Ferreri, V.S. Calderon, R. Esacobar Galindo, Silver activation on thin films of Ag–ZrCN coatings for antimicrobial activity: Mater. Sci. Eng C 55 (2015) 547–555.
16. C.R. Mariappan, N. Ranga, Influence of silver on the structure, dielectric and antibacterial effect of silver-doped bioglass-ceramic nanoparticles: Ceramics International 43 (2017) 2196–2201.
17. Rita Rebelo, V.S. Calderon, Raul Fangueiro, Influence of oxygen content on the antibacterial effect of Ag-O coatings deposited by magnetron sputtering: Surface & Coatings Technology 305 (2016) 1–10.
18. J. H. Kim, D. Buechel, T. Nakano, J. Tominaga, N. Atoda, Magneto-optical disk properties enhanced by a nonmagnetic mask layer: Appl. Phys. Lett. 77 (2000) 1774.
19. J. Kim, H. Fuji, Y. Yamakama, Takashi Nakano, Magneto-Optical Characteristics Enhanced by Super Resolution Near Field Structure: Jpn. J. Appl. Phys. 40 (2001) 1634–1636.
20. Y. Her, Y. Lan, W. Hsu, Effect of constituent phases of reactively sputtered AgOx film on recording and readout mechanisms of super-resolution near-field structure disk: Journal of Appl. Phys. 96 (2004) 1283–1288.
21. Z. S. Hu, F. Y. Hung, K. J. Chen, Recovery of thermal degraded ZnO photodetector by embedding nano-silver oxide nanoparticles: Applied Surface Science 279 (2013) 31–35.
22. D. Büchel, C. Mihalcea, T. Fukaya, Sputtered silver oxide layers for surface-enhanced Raman spectroscopy: Applied Physics Letters 79 (2001) 620–622.
23. J. Turner, Electrolytic studies on the system $Ag/Ag_2O/AgO$ in alkaline chloride solutions: Journal of Applied Electrochemistry 7 (1977) 369-378.
24. X. Zhang, S. Stewart, D. W. Shoesmith, Interaction of Aqueous Iodine Species with Ag_2O/Ag surfaces: J. Electrochem. Soc. 154 (2007) 70-76.
25. Sheela Berchmans, Amay J. Bandodkar, Wenzhao Jia, An Epidermal alkaline rechargeable Ag-Zn printable tattoo battery for wearable electronic: J. Mater. Chem. A 2 (2014) 15788-15795.
26. Makram A. Fakhri, Annealing Effects on Opto-electronic Properties of Ag_2O Films growth using Thermal Evaporation Techniques: Int. J. Nanoelectronics and Materials 9 (2016) 93-102.
27. A. C. Nwanya, P. E. Ugwuoke, B. a. Ezekoye, Structural and Optical Properties of Chemical Bath Deposited Silver Oxide Thin Films: Role of Deposition Time: Advances in Materials Science and Engineering 8 (2013) 450820.

28. Alex.1. Oje, A.A. Ogwu, M. Mirzaeian, Nathaniel Tsendzughul, Electrochemical energy storage of silver and silver oxide thin films in an aqueous NaCl electrolyte: Journal of Electroanalytical Chemistry 829 (2018) 59–68.
29. Mojtaba Mirzaeian, A.A. Ogwu, Nathaniel Tsendzughul, Surface characteristics of silver oxide thin film electrodes for supercapacitor applications: Colloids and Surfaces A: Physicochem. Eng. Aspects 519 (2017) 223–230.
30. P. Narayana Reddy, M. Hari Prasad Reddy, J. F. Pierson, Characterization of silver oxide thin films formed by reactive RF sputtering at different substrate temperature: ISRN Optics 7 (2014) 684317.
31. A. H. Hammad, M. SH. Abdel-Wahab, A. Alshahrie: Structural and morphological properties of sputtered silver oxide thin films: the effect of thin film thickness: Digest Journal of Nanomaterials and Biostructures 11 (2016) 1245-1252.
32. M. Hari Prasad Reddy, S. Uthanna, Substrate temperature influenced structural and optical properties of RF magnetron sputtered pure and copper doped silver oxide thin films: IJCRGG ISSN 7 (2015) 1079-1084.
33. Xiaolong Zhao, Yongning He, Wenbo Peng, Electrical and optical characterization of AgOx films deposited by RF reactive magnetron sputtering: Thin Solid Films 636 (2017) 333–338.
34. B. Ingham, M. F. Toney, Metallic films for electronic, optical and magnetic applications: Structure, Processing and Properties: 2013 first edition pp 3-38.
35. M. F. Al-Kuhaili, Characterization of thin films produced by the thermal evaporation of silver oxide: Journal of Physics D 40 (2007) 2847–2853.
36. Rita Rebelo, N.K. Manninen, Luísa Fialho, Morphology and oxygen incorporation effect on antimicrobial activity of silver thin films: Applied Surface Science 371 (2016) 1–8.
37. Kalyanaraman Kalpana, Vaithilingam Selvaraj, A novel approach for the synthesis of highly active ZnO/TiO2/Ag_2O nanocomposite and it's photocatalytic applications: Ceramics International 41(2015) 9671–9679.
38. Hamid Entezar Mehdi. M.R. Hantehzadeh, Shahoo Valedbagi, Physical properties of silver oxide thin film prepared by dc magnetron sputtering: effect of oxygen partial pressure during growth: J. Fusion Energy 32 (2013) 28–33.
39. Geoffrey I. N. Waterhouse, The thermal decomposition of silver (I, III) oxide a combined XRD, FT-IR and Raman spectroscopic study: Phys. Chem. Chem. Phys. 3 (2001) 3838-3845.
40. Geoffrey I.N. Waterhouse, Graham A. Bowmaker, James B. Metson, Oxygen chemisorption on an electrolytic silver catalyst a combined TPD and Raman spectroscopic study: Applied Surface Science 214 (2003) 36–51.

41. Irene Martina, Rita Wiesinger, Micro-Raman characterisation of silver corrosion products: Instrumental set up and reference database 9 (2012) 1-8.
42. G. Alagumuthu, R. Kirubha, Synthesis and characterisation of silver nanoparticles in different medium: Open Journal of Synthesis Theory and Applications 1 (2012) 13-17.
43. M. Rafiq H. Siddiqui, S.F. Adil, M.E. Assal, Synthesis and characterization of silver oxide and silver chloride nanoparticles with high thermal Stability: Asian Journal of Chemistry 25 (2013) 3405-3409.
44. Mahendra Kumar Trivedi1, Rama Mohan Tallapragada1, Alice Branton, The Potential Impact of biofield energy treatment on the physical and thermal properties of silver oxide powder: International Journal of Biomedical Science and Engineering 3 (2015) 62-68.
45. Kamyar Shameli, Mansor Bin Ahmad, Seyed Davoud Jazayer, Synthesis and characterization of polyethylene glycol-mediated silver nanoparticles by the green method: Int. J. Mol. Sci. 13 (2012) 6639-6650
46. Tiffany C. Kaspar, Tim Droubay, Scott A. Chambers, Paul S. Bagus, Spectroscopic evidence for Ag (III) in highly oxidized silver films by X-ray photoelectron spectroscopy: J. Phys. Chem. C 114 (2010) 21562–21571.
47. Xiao-Yong Gao, Song-You Wang, Jing Li, Yu-Xiang Zheng, Study of structure and optical properties of silver oxide films by ellipsometry, XRD and XPS methods: Thin Solid Films 455 –456 (2004) 438–442.
48. Weifeng Wei, Xuhui Mao, Luis A. Ortiz, Donald R. Sadoway, Oriented silver oxide nanostructures synthesized through a template-free electrochemical route: Journal of material chemistry 21 (2010) 432-438.
49. F. Paladini, R.A. Picca, M.C. Sportelli, N. Cioffi, Surface chemical and biological characterization of flax fabrics modified with silver nanoparticles for biomedical applications: Materials Science and Engineering C 52 (2015) 1–10.
50. Ana Maria Ferraria, Ana Patrícia Carapeto, Ana Maria Botelho do Rego, X-ray photoelectron spectroscopy: Silver salts revisited: Vacuum 86 (2012) 1988-1991.
51. Jason F. Weaver, Gar B. Hoflund Surface Characterization Study of the Thermal Decomposition of Ag_2O: Chem. Mater. 6 (1994) 1693–1699.
52. Souvik Agasti, Avijit Dewasi, Anirban Mitra, Structural and optical properties of pulse laser deposited Ag_2O thin films: AIP Conference Proceedings 1953 (2018) 060001.
53. J. Wei, N Nagarajan, I. Zhitomirsky, Manganese oxide films for electrochemical supercapacitors: Journal of Materials Processing Technology 186 (2007) 356–361.

54. P. Staiti, F. Lufrano, Study and optimization of Manganese oxide-based electrodes for electrochemical supercapacitors: Journal of power sources 187 (2009) 284-289.
55. Yong Zhang, Guang-yin Li, Yan Lv, Li-zhen Wang, Electrochemical investigation of MnO_2 electrode material for supercapacitors: International journal of hydrogen energy 36 (2011) 11760 – 11766.
56. J. Keraudy, J. García Molleja, A. Ferrec, B. Corraze, Structural, morphological and electrical properties of nickel oxide thin films deposited by reactive sputtering: Applied Surface Science 357 (2015) 838–844.
57. Youyi Sun, Wenhui Zhang, Diansen Lib, Direct formation of porous MnO_2/Ni composite foam applied for high-performance supercapacitors at mild conditions: Electrochimica Acta 178 (2015) 823–828.
58. Ma Jiao-Min, Liang Yan, Gao Xiao-Yong, Effect of substrate temperature on microstructure and optical properties of single-phased Ag_2O film deposited by using radio-frequency reactive magnetron sputtering method: Chin. Phys. B 20 (2011) 056102.
59. Thokozani Xaba, Makwena J. Moloto, Mundher Al-Shakban, The effect of temperature on the growth of Ag2O nanoparticles and thin films from bis(2-hydroxy-1-naphthaldehydato) silver(I) complex by the thermal decomposition of spin-coated films: Materials Science in Semiconductor Processing 71 (2017) 109–115.
60. R. Dimitrijević, O. Cvetković, Z. Miodragović, SEM/EDX and XRD characterization of silver nanocrystalline thin film prepared from organometallic solution precursor: J. Min. Metall. Sect. B-Metall. 49 (2013) 91 – 95.
61. Souvik Agasti, Avijit Dewasi, Anirban Mitra, Structural and optical properties of pulse laser deposited Ag_2O thin films: AIP Conference Proceedings 1953 (2018) 060001.
62. Jalal Arjomandi, Jin Yong Lee, Raheleh Movafagh, Polyaniline/aluminum and iron oxide nanocomposites supercapacitor electrodes with high specific capacitance and surface area: Journal of Electroanalytical Chemistry 810 (2018) 100–108.
63. S. W. Zhang, G. Z. Chen. Manganese oxide-based materials for supercapacitors: Energy Materials 3 (2008)186-200.
64. Huaping Zhao, Long Liu, Ranjith Vellacheri, Recent advances in designing and fabricating self-supported nanoelectrodes for supercapacitors: Adv. Sci. 4 (2017) 1700188.
65. Sara L. Schellbach, Sergio N. Monteiro, Jaroslaw W. Drelich, A novel method for contact angle measurements on natural fibers: Materials Letters 164 (2016) 599–604.
66. R. Belibel, C. Barbaud, L. Mora, Dynamic contact angle cycling homogenizes heterogeneous surfaces: Materials Science and Engineering C 69 (2016) 1192–1200.

67. C.W. Extrand, Uncertainty in contact angle estimates from Wilhelmy tensiometer: Journal of Adhesive Science and Technology 29 (2015) 2515-2520.
68. Hongyun Chen, Fazhi Zhang, Tao Chen, Comparative analysis of the dynamic contact angles for two types of superhydrophobic layered double hydroxide film surfaces: Chemical Engineering Science 64 (2009) 2957-2962.
69. R. K. Roy, H. W. Choi, S. K. Park, K. R. Lee, Surface energy of the plasma-treated Si incorporated diamond-like carbon films: Diamond and Related Materials 16 (2007) 1732-1738.
70. Sambhaji M. Pawar, Multi-functional reactively sputtering copper oxide electrodes for supercapacitor and electro-catalyst in direct methanol fuel applications: Scientific Reports 6 (2016) 21310.
71. Chun Huang, Solid-state supercapacitors with rationally designed heterogeneous electrodes fabricated by large area spray processing for wearable energy storage applications: Scientific Reports 6 (2016) 25684.
72. Recep Yuksela, Ece Alpuganc, Husnu Emrah Unalana, Coaxial silver nanowire/polypyrrole nanocomposite supercapacitors: Organic Electronics 52 (2018) 272–280
73. Junyan Liu, Tinghui Jiang, Feng Duan, Electrophoresis deposition of flexible and transparent silver nanowire/graphene composite film and its electrochemical properties: Journal of Alloys and Compounds 745 (2018) 370-377.
74. C. Criado, P. GalÃ¡n-Montenegro, P. VelÃ¡squez, Diffusion with general boundary conditions in electrochemical systems: Journal of Electroanalytical Chemistry 488 (2000) 59–63.
75. Sachin A. Pawar, Dipali S. Patil, Jae Cheol Shin, Electrochemical battery-type supercapacitor based on chemosynthesized Cu_2S-Ag_2S composite electrode: Electrochimica Acta 259 (2018) 664-675.
76. Jian-Yang Lin, Jung-Jie Huang, Yu-Lee Hsueh, Diameter effect of silver nanowire doped in activated carbon as thin film electrode for high-performance supercapacitor: Applied Surface Science 477 (2019) 257–263.
77. Adriana Ispas, Manuel Pölleth, Khanh Hoa Tran Ba, Electrochemical deposition of silver from 1-ethyl-3-methylimidazolium Trifluoromethanesulfonate: Electrochimica Acta 56 (2011) 10332– 10339.
78. Ming-Chih Tsai, Ding-Xuan Zhuang, Po-Yu Chen, Electrodeposition of macroporous silver films from ionic liquids and assessment of these films in the electrocatalytic reduction of nitrate: Electrochimica Acta 55 (2010) 1019–1027.

79. Sherif Zein El Abedin, F. Endres, Electrodeposition of nanocrystalline silver films and nanowires from the ionic liquid 1-ethyl-3-methylimidazolium trifluoromethylsulfonate: Electrochimica Acta 54 (2009) 5673–5677.
80. Y. Ben Amor, E. Sutter, H. Takenouti, Electrochemical study of the tarnish layer of silver deposited on glass: Electrochimica Acta 131 (2014) 89–95.
81. S.M. Pawar, A.I. Inamdar, K.V. Gurav, Effect of oxidant on the structural, morphological and supercapacitive properties of nickel hydroxide nanoflakes electrode films: Materials Letters 141 (2015) 336–339.
82. Elanthamilan Elaiyappillai, Sakthivel Kogularasu, Shen-Ming Chen, Muthumariappan Akilarasan, Sonochemically recovered silver oxide nanoparticles from the wastewater of photo film processing units as an electrode material for supercapacitor and sensing of 2, 4, 6-trichlorophenol in agricultural soil samples: Ultrasonics - Sonochemistry 50 (2019) 255–264.
83. Jung Hoon Chae, George Zheng Chen, Influences of ions and temperature on performance of carbon nano-particulates in supercapacitors with neutral aqueous electrolytes: Particuology 15 (2014) 9–17.
84. Alexander J. Roberts, Robert C.T. Slade, Effect of specific surface area on capacitance in asymmetric carbon/α-MnO_2 supercapacitors: Electrochimica Acta 55 (2010) 7460–7469.